Characterizing and monitoring fault structures

Chantal van Dinther[1], Andres Barajas[1], Shujuan Mao[2,1]
Qingyu Wang[1,2], Bérénice Froment, Florent Brenguier[1],
Ludovic Margerin[3],…. Michel Campillo[1]

1: ISTerre, Grenoble
2:MIT, Boston
3:IRAP, Toulouse

European Research Council erc
F-IMAGE
Seismic functional imaging of the brittle crust.

UNIVERSITÉ Grenoble Alpes

irap astrophysique & planétologie

ISTerre Institut des Sciences de la Terre

EAPS Earth, Atmospheric and Planetary Sciences

1-Introduction
2-Present day limitations and assumptions
3-Examples of applications
4-Imaging and 2D kernels
5-Non-uniform scattering
6-Depth dependance and the coupling of surface waves and body waves

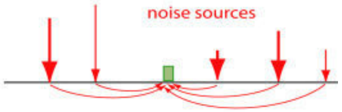

Noise - seismic waves emitted by random ambient sources

includes also coda waves although ballistic waves are dominant in most cases

Ambient noise seismology

Constructing virtual sismograms between 2 sensors **?**

A mathematical argument: under specific conditions on the sources S of the ambient noise, the correlation between records at 2 points P1 et P2 produces the Green function between the 2 points.

$$Im(G(P1, P2; \omega)) \approx i\omega \langle G(S, P1; \omega).\, G(S, P2; \omega)^* \rangle_{\text{sources S}}$$

correlation

Im(G) represents the causal (t) and acausal (-t) contributions

-If the field has been fully randomized by multiple scattering

-If the ‘noise’ results from a uniform distribution of sources in the volume (e.g. Y. Colin de Verdière)

-Approximations to representation theorems (e.g. K. Wapenaar) ➔ uniform sources on the boundary

- Analogy with time reversal mirors (Derode et al., 2003).

Noise based seismic velocity temporal changes

Because seismic noise records is continuous in time, it is possible to reconstruct **repeating virtual seismic sources** and perform **continuous monitoring of seismic velocities**, from the beginning of the recording.

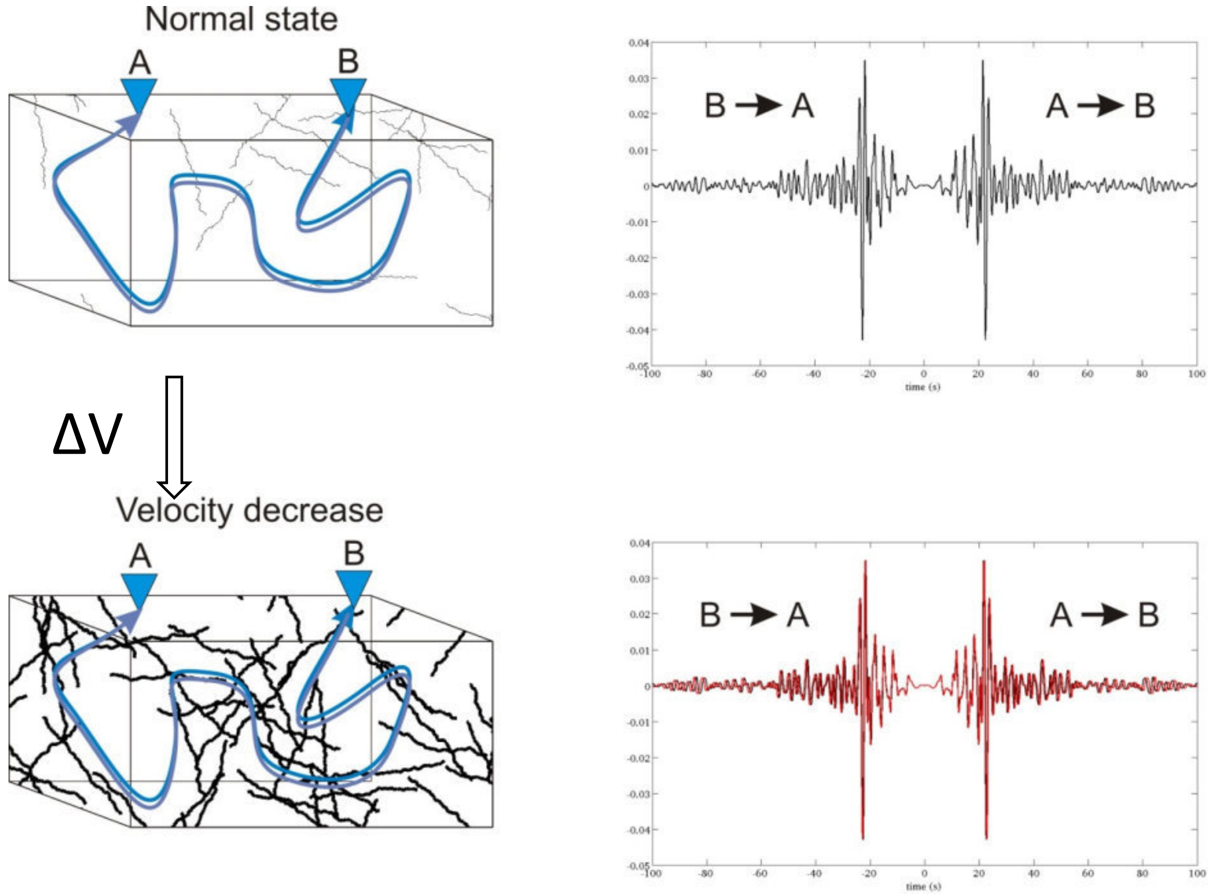

1-Introduction

2-Present day limitations and assumptions

3-Examples of applications

4-Imaging and 2D kernels

5-Non-uniform scattering

6-Depth dependance and the coupling of surface waves and body waves

Correlation functions as approximate Green functions

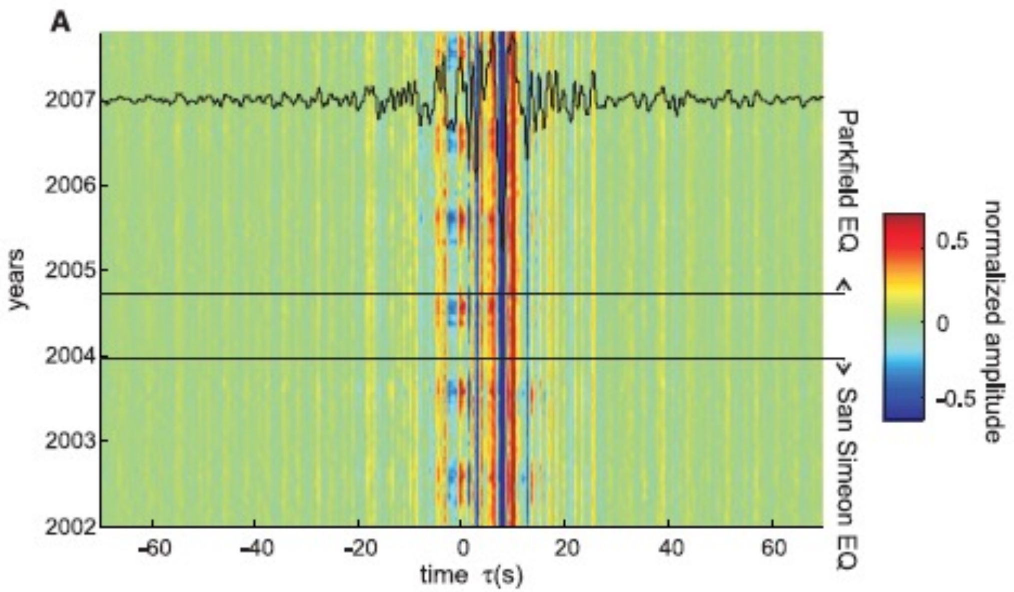

Direct waves are sensitive to noise source distribution (errors small enough for tomography)
Relative stability of the 'coda' of the noise correlations.

Importance of the analysis of the ambient noise structure

1- Reconstruction of direct waves from direct waves from distant sources

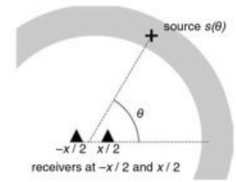

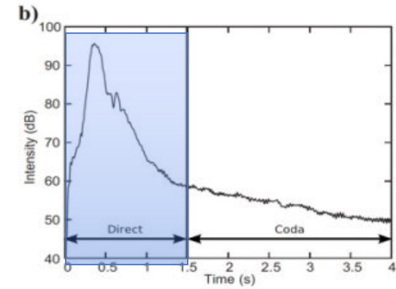

Field data: Bias in the travel time due to anisotropic intensity of noise field

Increasing anisotropy of the source intensity *B*

Azimuthal distribution of source intensity

Travel time error wrt the observed Green function

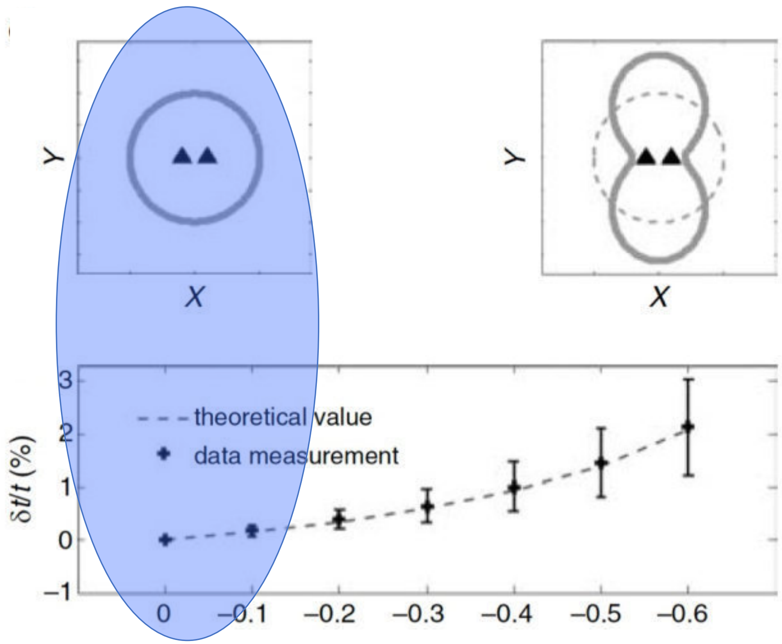

$$B(\theta) = 1 + B_2 \cos(2\theta)$$

$$\delta t = \frac{1}{2t\,\omega_0^2 B(0)} \left. \frac{d^2 B(\theta)}{d\theta^2} \right|_{\theta=0}$$

valid with t (travel time) > T (period)

2-Reconstruction of direct waves from scattered waves

-isotropy improved by multiple scattering

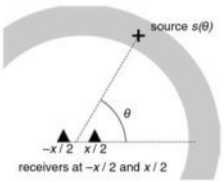

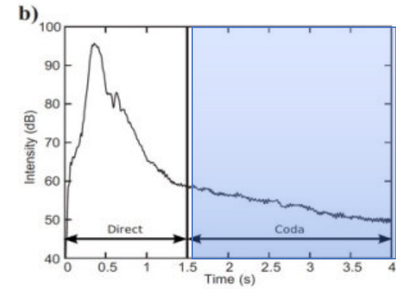

Increasing anisotropy of the source intensity *B*

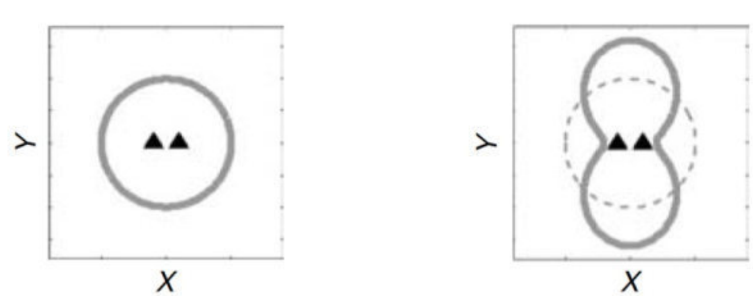

$$B(\theta) = 1 + B_2 \cos(2\theta)$$

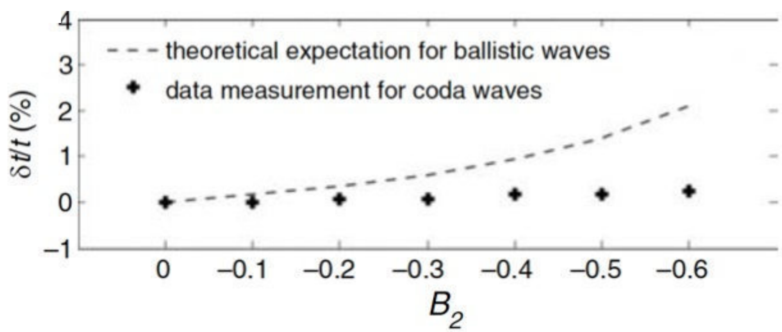

No visible bias in the correlation of coda waves!

From Froment, Campillo, Roux, Gouédard, Verdel and Weaver 2011.

2-Reconstruction of direct waves from scattered waves

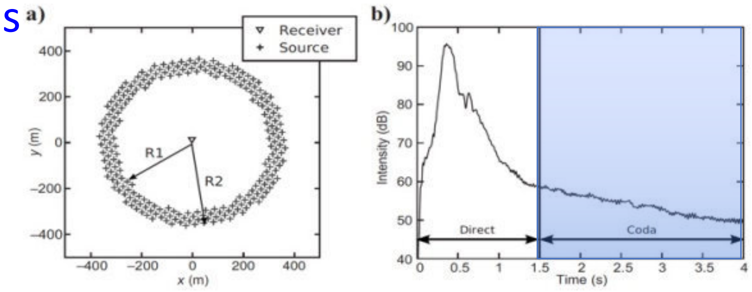

Correlation of coda waves

-isotropy provided by multiple scattering

Increasing anisotropy of the source intensity *B*

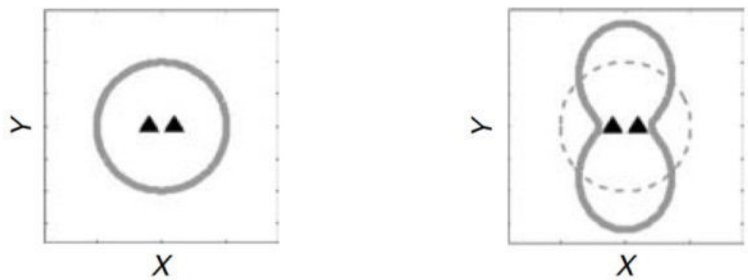

$$B(\theta) = 1 + B_2 \cos(2\theta)$$

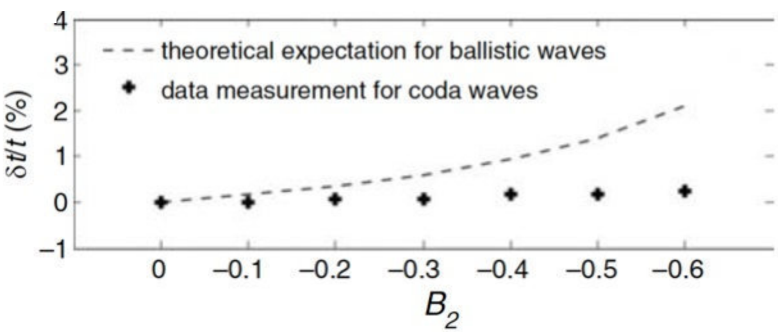

Scattering provides the diversity of incidence directions ➔isotropization of intensity

No bias in the correlation of coda waves!

Noise records contain direct **<u>and</u>** scattered waves: the separation is usually impossible

➔ the biases of direct wave travel times are generally small enough for imaging purpose

➔ Importance of processing strategies: equalization, filtering, C3, ….

3-Reconstruction of coda waves

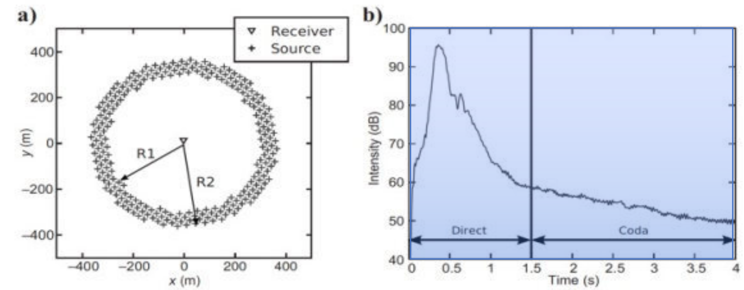

Measuring slight changes of seismic velocity using coda waves (long travel time)

Numerical simulations in a scattering medium with strong anisotropic intensity of sources (2D spectral elements)

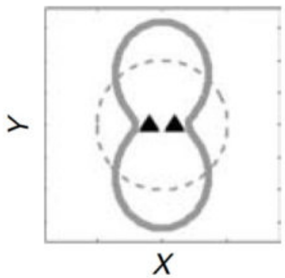

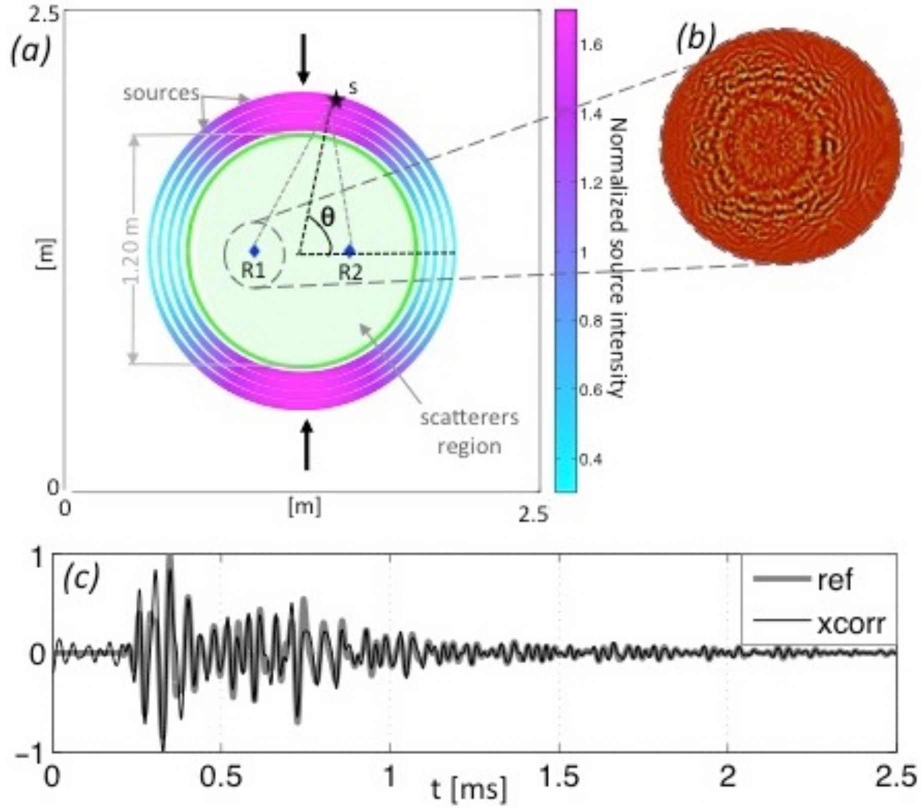

Comparison of correlations with Green function

Colombi et al., 2014

Measure of the bias induced by a strong anisotropy of the noise wave field (delay with respect to the Green function)

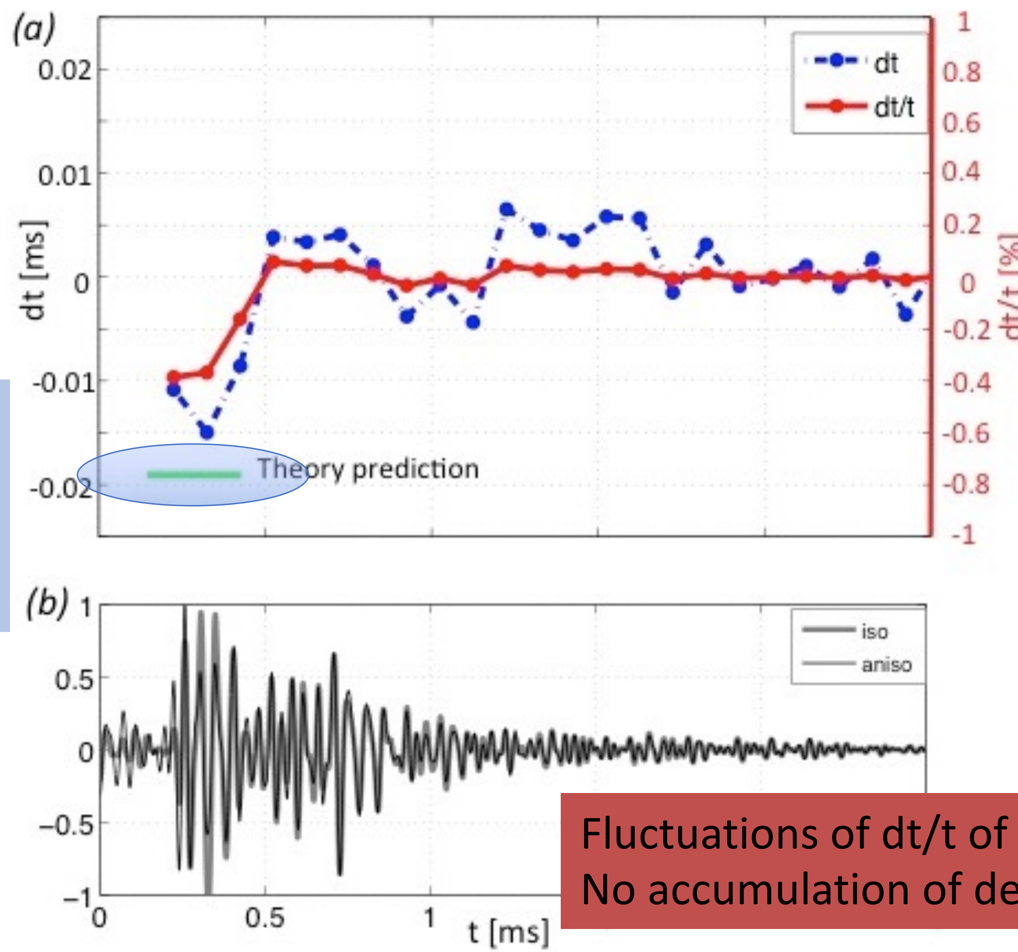

Theoretical prediction of the relative delay for the direct wave in an homogeneous body (Froment et al., 2010)

Blue: delay

Red: relative delay

Fluctuations of dt/t of the order of 10^{-4}
No accumulation of delay with lapse time

Colombi et al., 2014

➔ use of the coda of noise correlations

1-Introduction
2-Present day limitations and assumptions
3-Examples of applications
4-Imaging and 2D kernels
5-Non-uniform scattering
6-Depth dependance and the coupling of surface waves and body waves

Application to the Parkfield earthquake *(Brenguier et al. 2008)*

Short period sensors / Processing in the period 1-10s

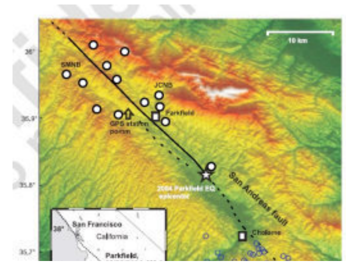

Assumption 0: Homogeneous change of seismic velocity : constant slope of δt

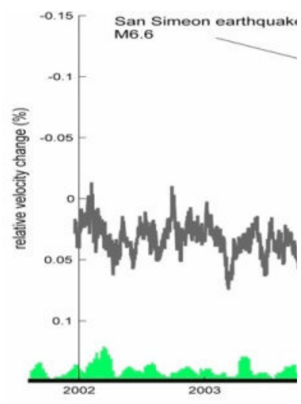

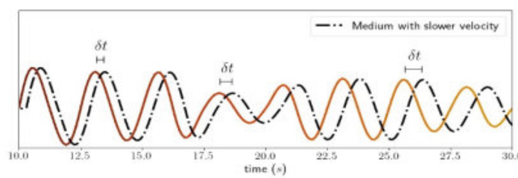

Two correlations at different dates

Coda - result of multiple scattering on random inhomogeneities

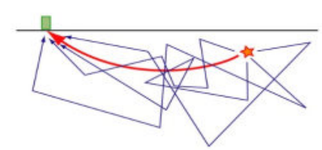

Poupinet et al,. 1984. (EQ doublets) later coda wave interferometry

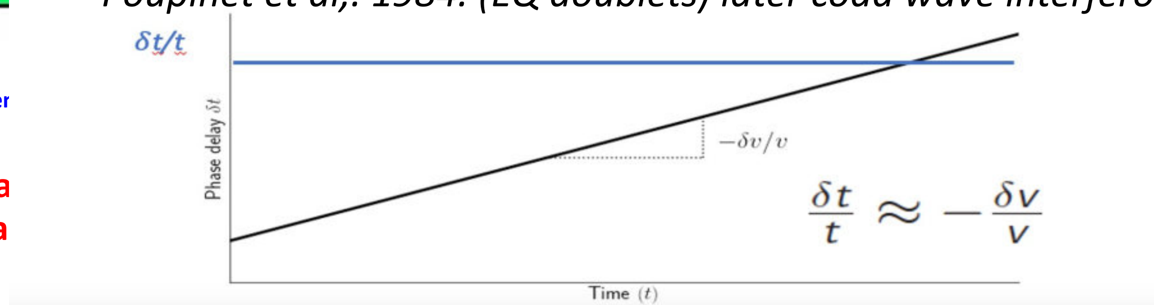

Distant ever

A lot of specta
environmenta

Do changes occur at depth ?

Evidence for shallow variations: known in soft sediments from seismic records
applications of continuous monitoring from noise

Evidences for deep changes:
SSE, Wenchuan
Japan after Tohoku
Direct observations at depth in a mine

Local scale: test with industrial noise

Velocity change due to blast and excavation in a mine

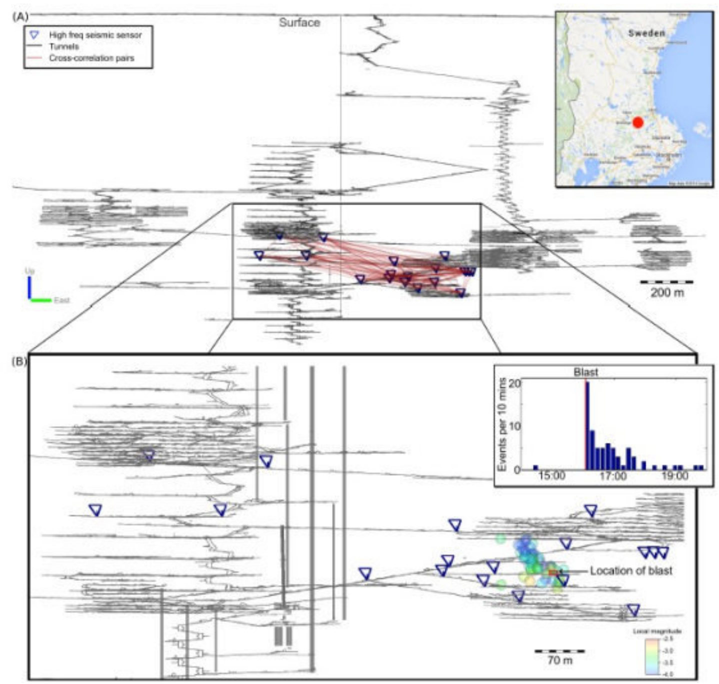

Use of the strong industrial noise in the mine.
Note the intense scattering associated with the tunnels.

Olivier et al., 2014

Noise based monitoring: Velocity change due to blast and excavation in a mine (body waves)

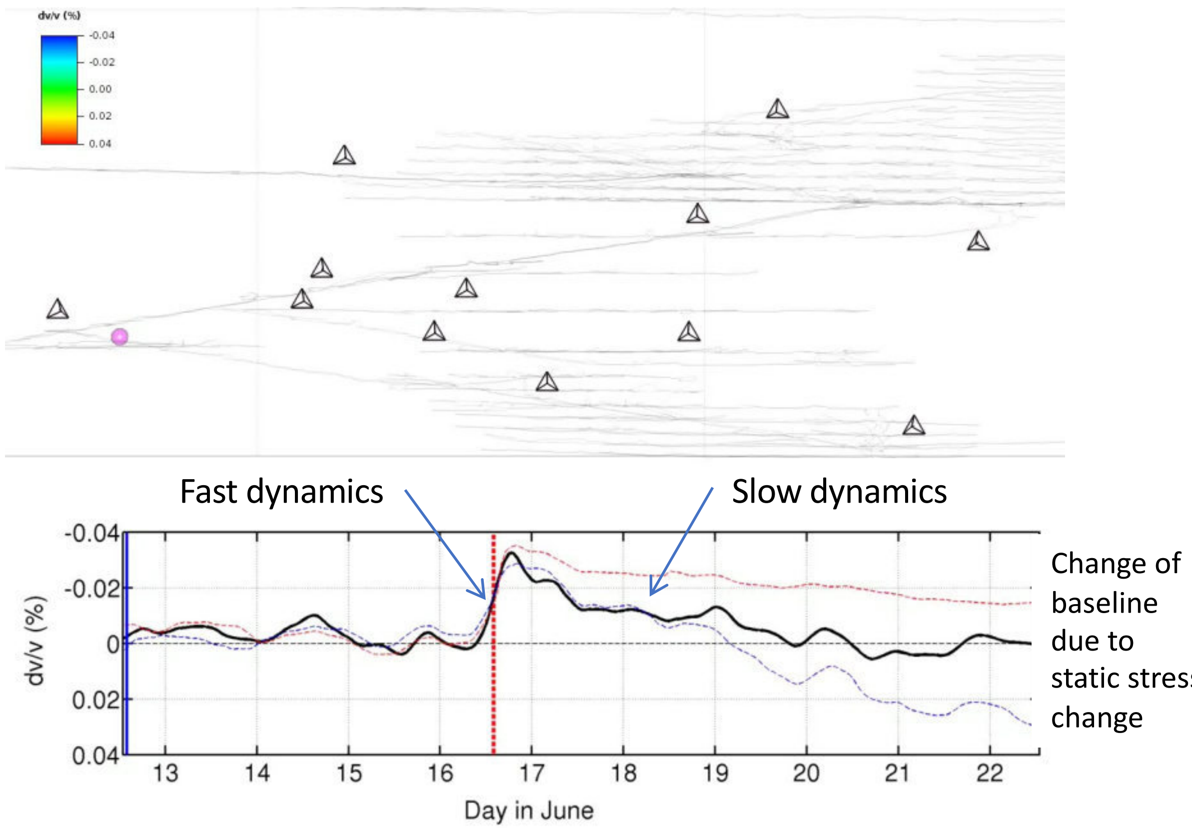

Olivier et al., 2014

Slow dynamics : Relaxation-aging (e.g. Amir et al., 2011 ; Snieder et al., 2017)

Comparison of velocity changes and volumetric stress changes

SLIDE VIEW

PLANE VIEW

Instaneous velocity drop

'Static' velocity change

Static stress change (model)

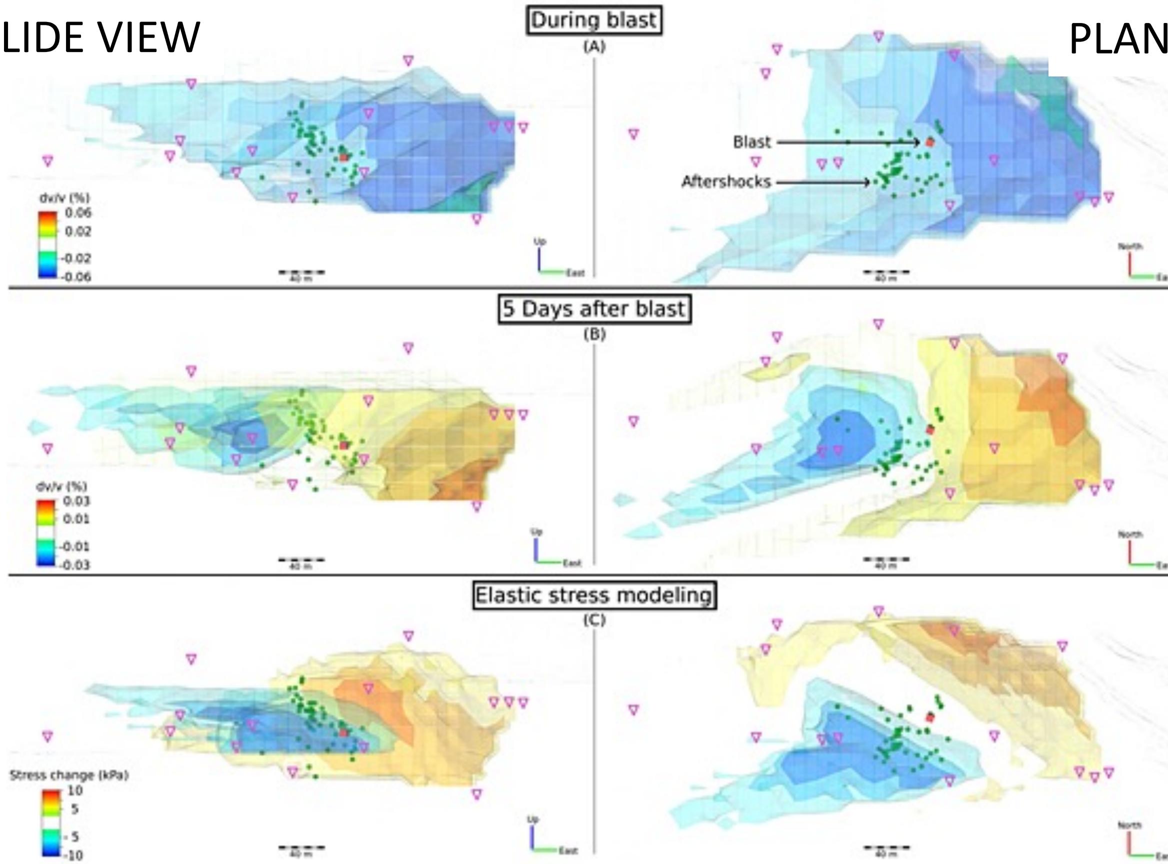

Frequency (depth) dependent spatial distribution of dv/v

Damage in the shallow crust

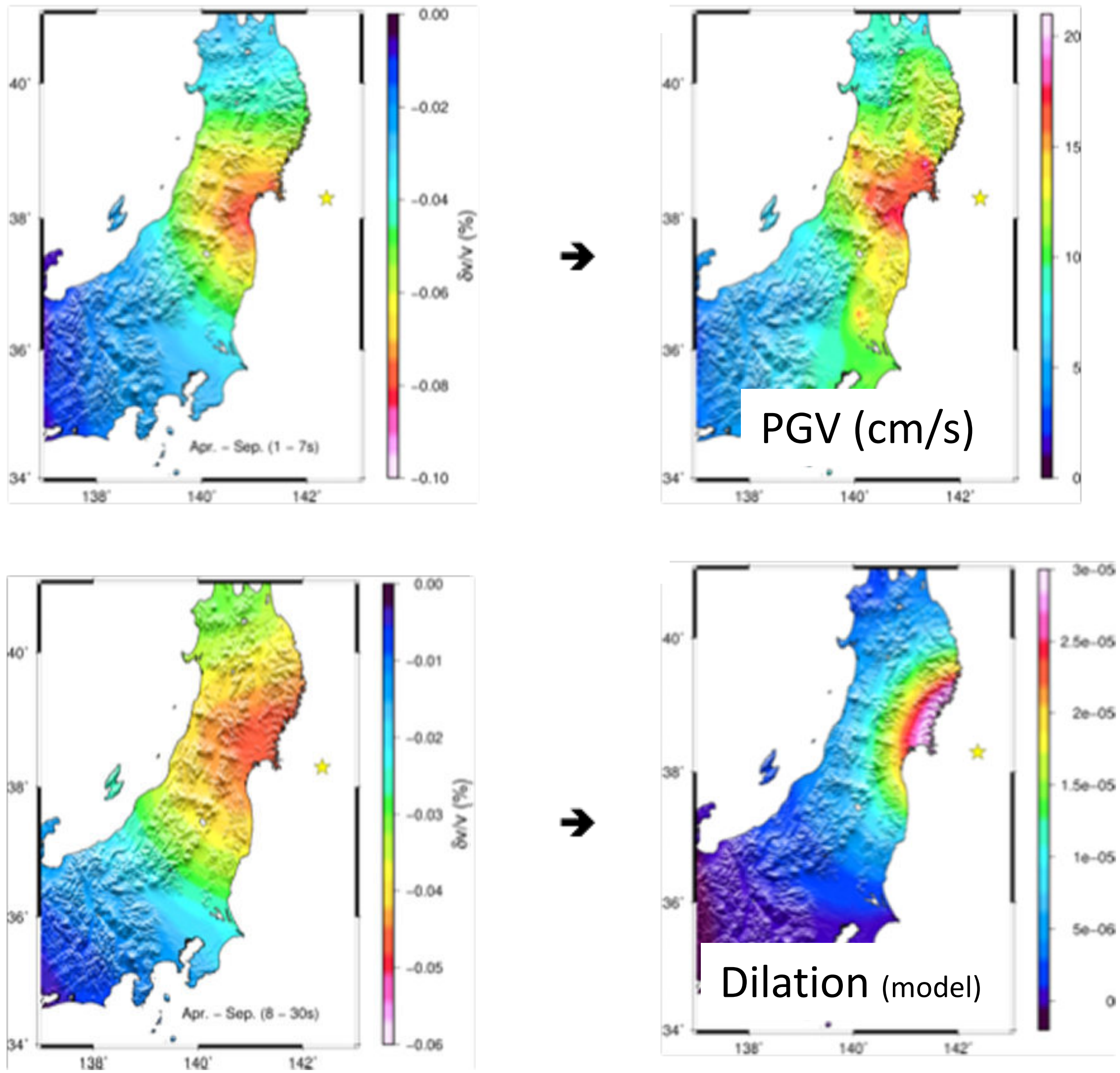

Strain from deep crust

From Wang et al., 2020

Frequency -depth- dependent temporal variation of dv/v

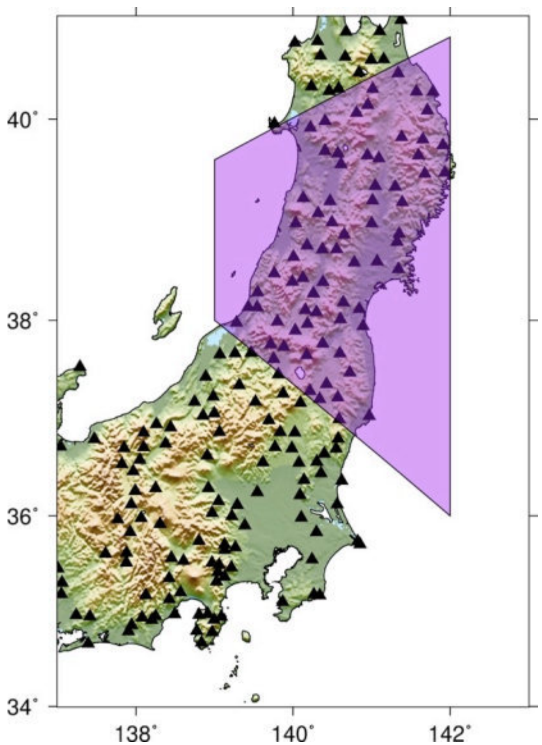

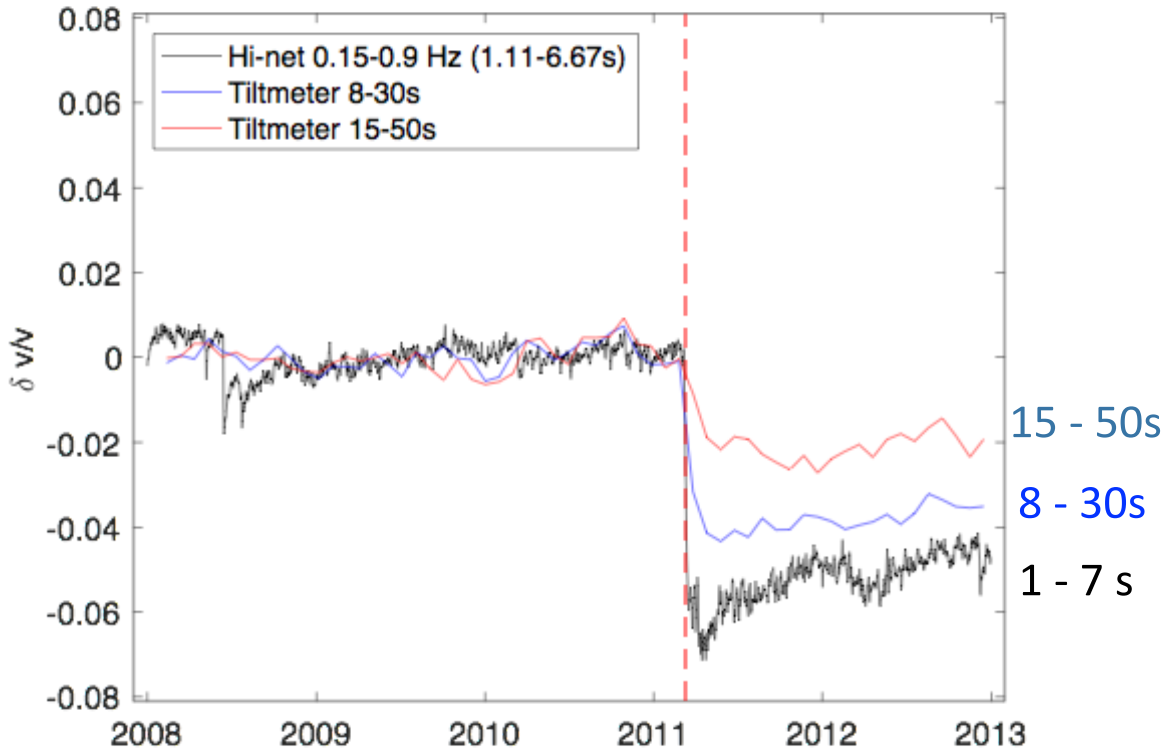

Period dependent delay of the response in time.

Fluids from below flowing through the volcanic range

Wang et al., 2020

1-Introduction
2-Present day limitations and assumptions
3-Examples of applications
4-Imaging and 2D kernels
5-Non-uniform scattering
6-Depth dependance and the coupling of surface waves and body waves

Coda=multiply scattered waves

Assumptions:

0: uniform change

1:uniform scattering properties

2: scalar waves

3: isotropic scattering

.....

Assumption 0: Homogeneous change of seismic velocity : constant slope of δt

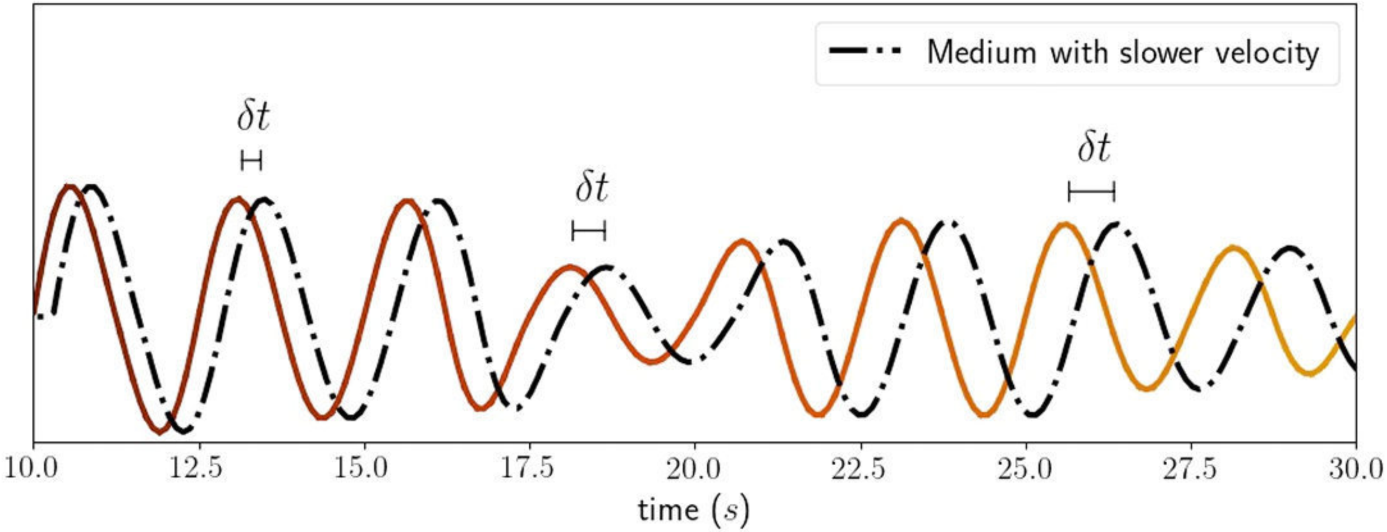

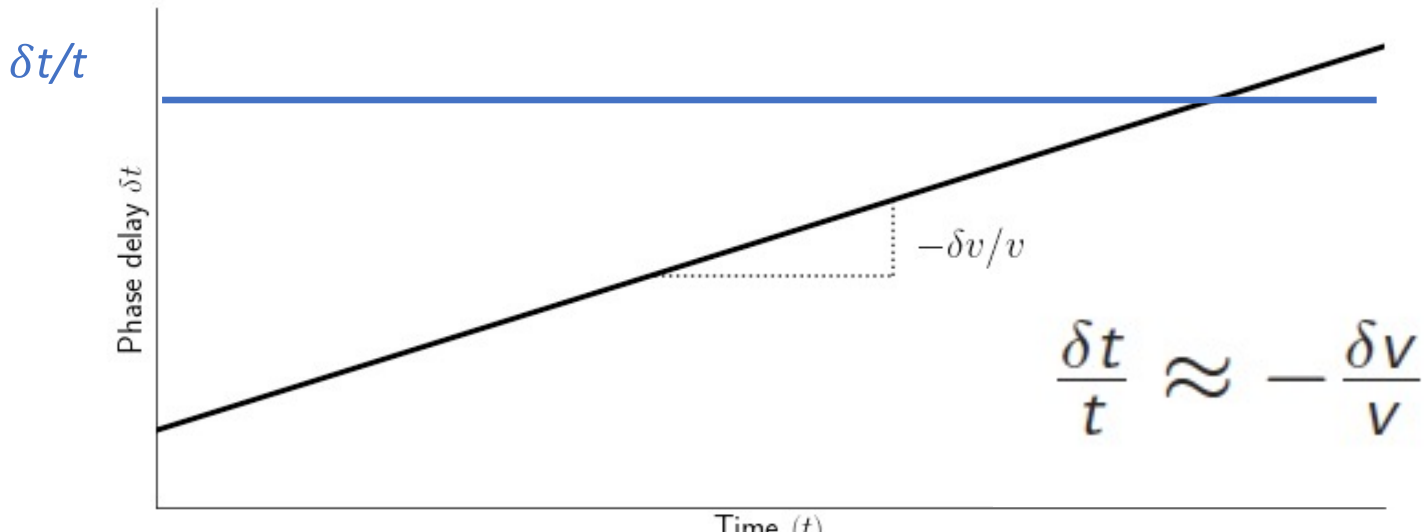

$$\frac{\delta t}{t} \approx -\frac{\delta v}{v}$$

Beyond assumption 0 : Localized change of seismic velocity / body waves

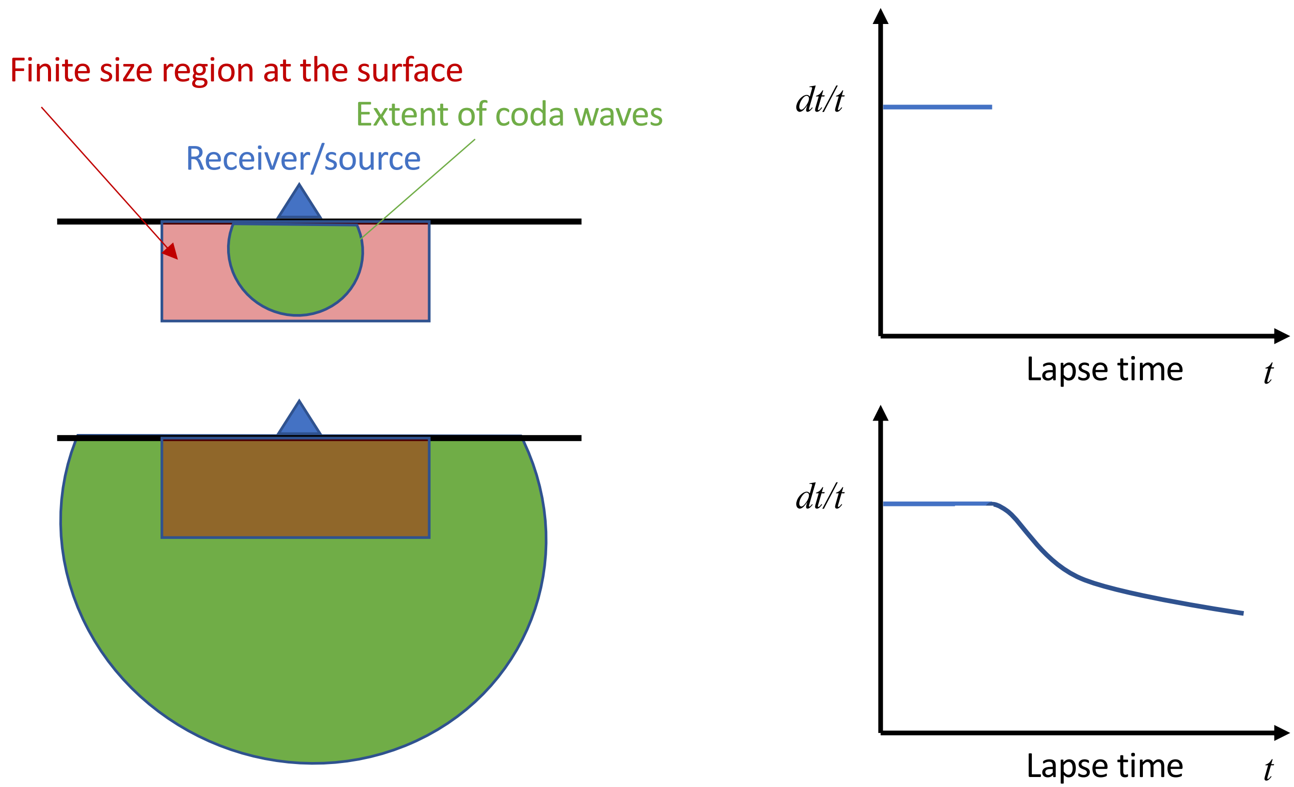

Actual meaning of the results under an homogeneous distribution hypothesis ?

Linear formulation

$$\delta t(\tau, r_1, r_2) = -\int_V K(x, r_1, r_2, \tau) \frac{\delta v}{v}(x)\, dV(x)$$

The sensitivity kernel relates the travel time with a spatial distribution. It can be calculated measuring the time the particles pass in each zone of the medium, when going from the source to the receiver in a given time

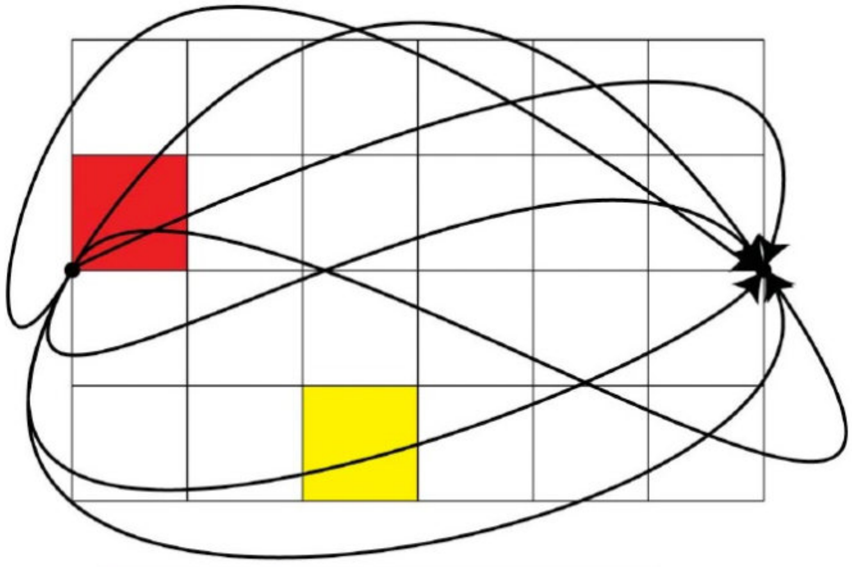

The detail of the subsurface are not known.

To perform differential imaging, we rely on statistical models of heterogeneity and solutions of the Radiative Transfer Equation.

Kernels for travel time K_{tt} (or amplitude K_Q *(absorption) : passive perturbations*

We made the assumption of isotropic scattering, but the field itself is highly anisotropic for finite times

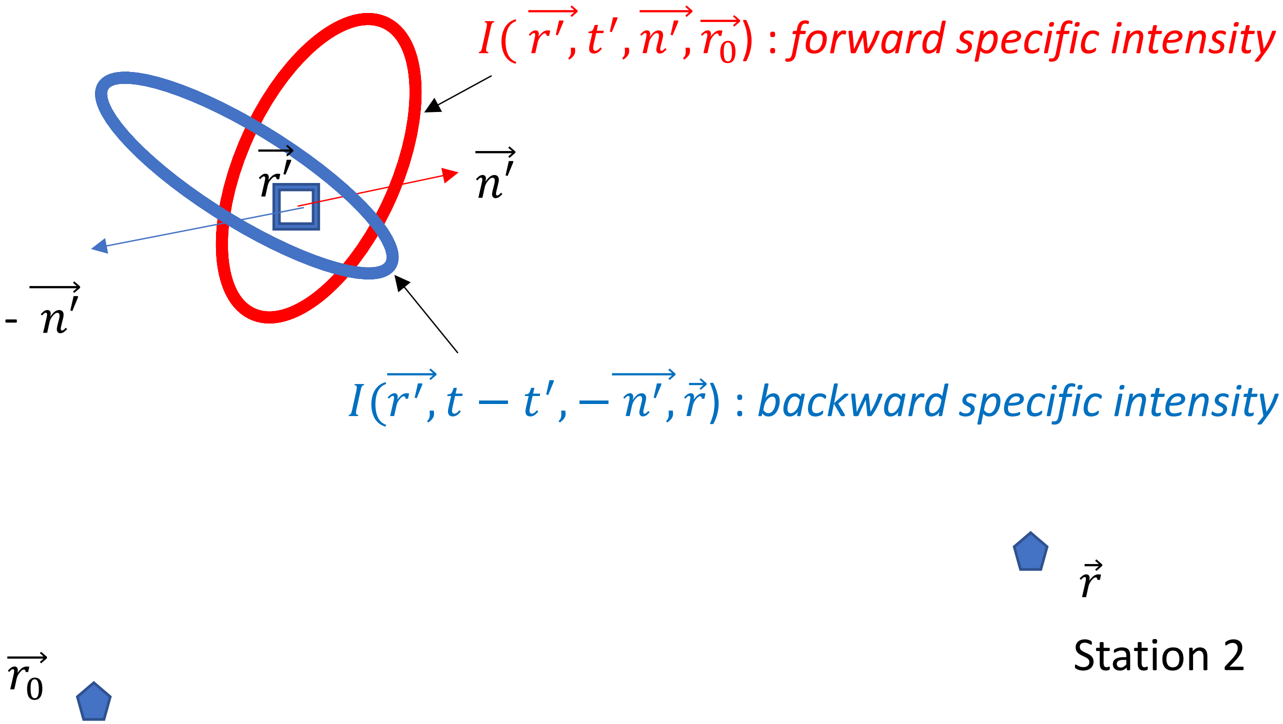

$$K_{tt}\left(\mathbf{r}', t; \mathbf{r}, \mathbf{r}_0\right) = S^D \int_0^t \int_{S^D} \frac{I\left(\mathbf{r}', t-t', -\mathbf{n}'; \mathbf{r}\right) I\left(\mathbf{r}', t', \mathbf{n}'; \mathbf{r}_0\right) dt' dn'}{I\left(\mathbf{r}, t; \mathbf{r}_0\right)}$$

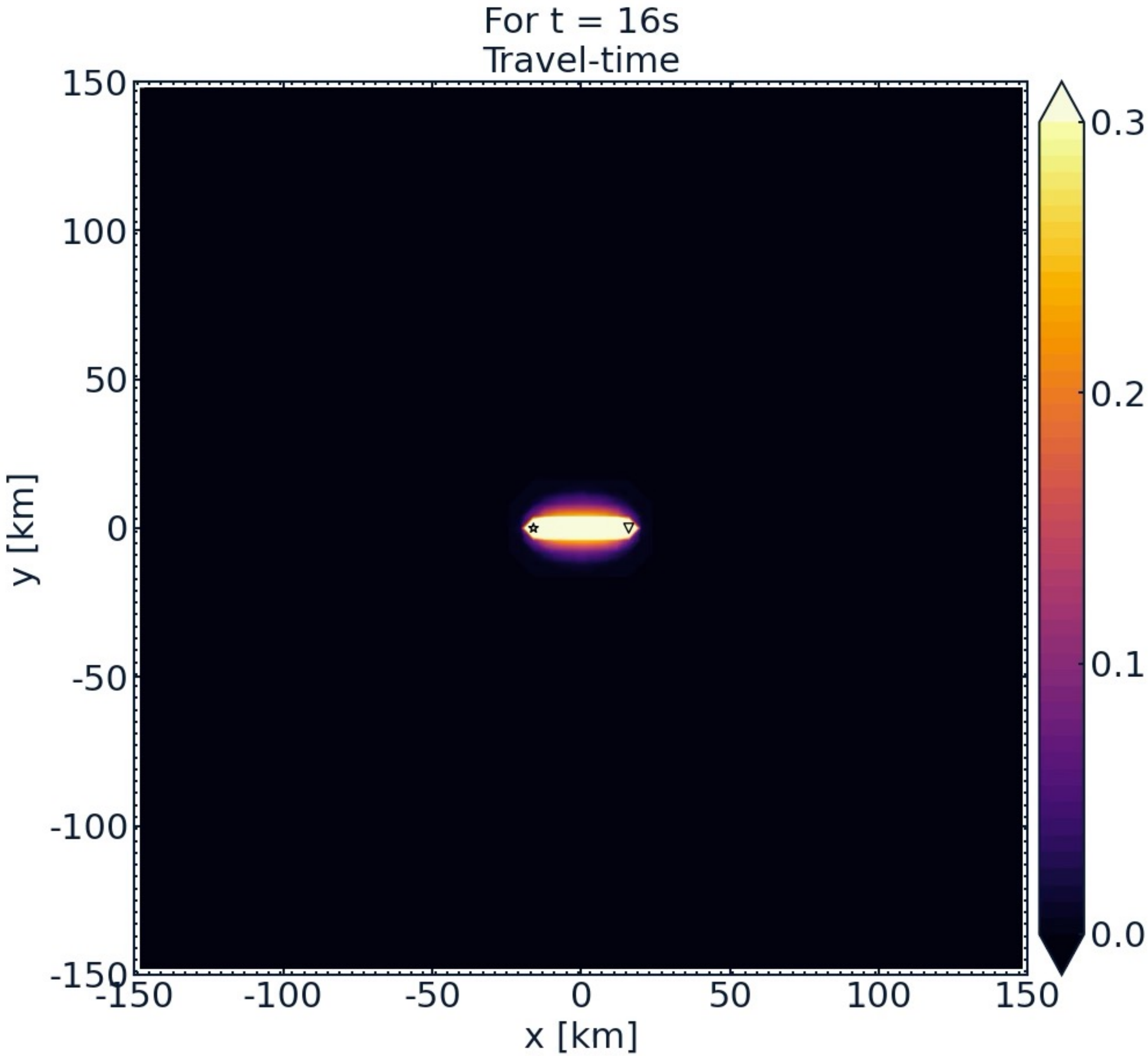

RTE Monte Carlo solution

Space-Time Monitoring of Groundwater Fluctuations via Passive Seismic Monitoring

Mao et al., 2022

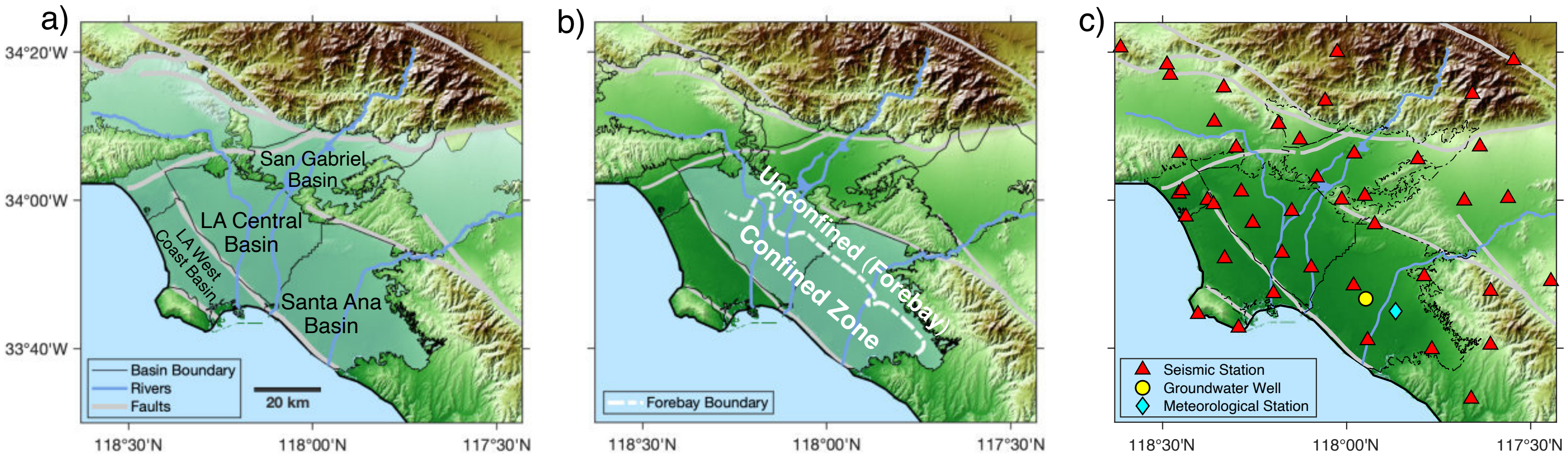

Maps of velocity changes using dv/V kernels

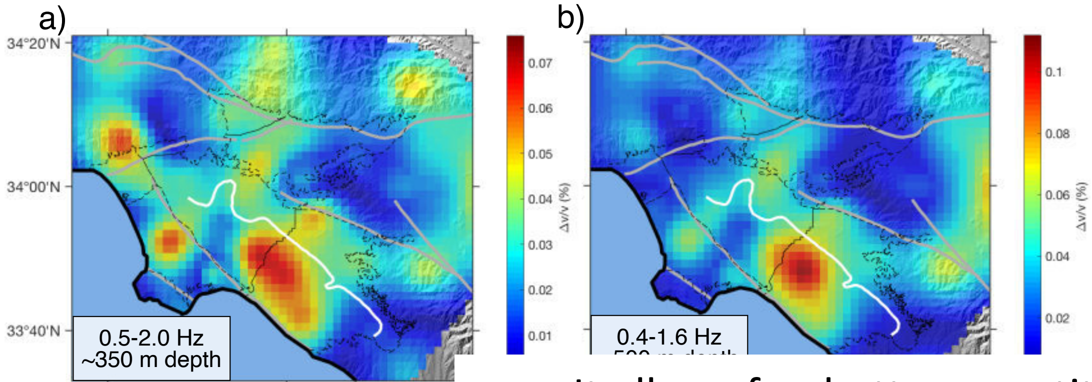

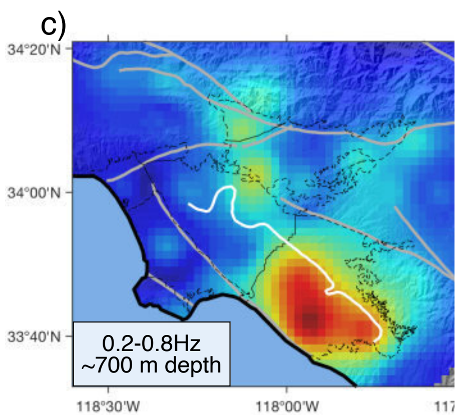

It allows for better quantitative measurements

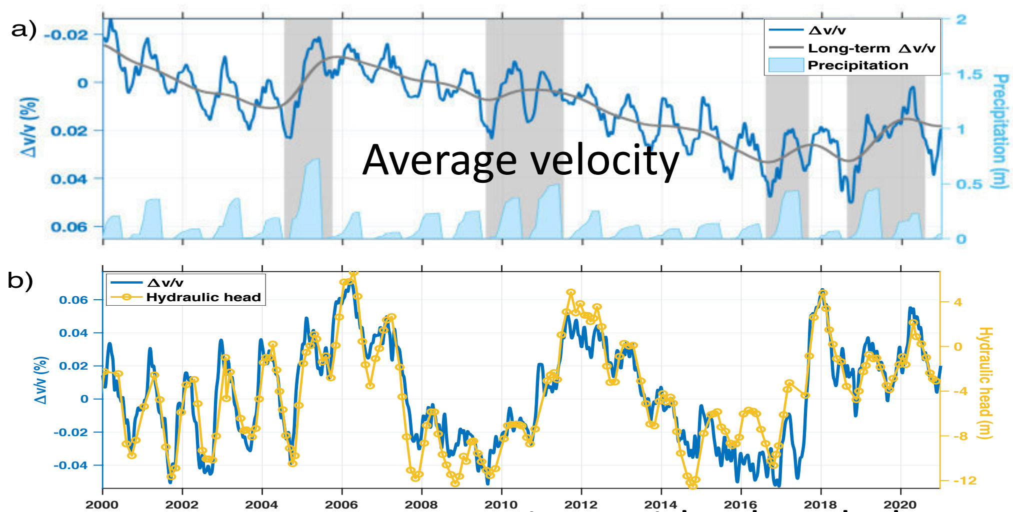

Comparison with a borehole measurement (no colocated station)

1-Introduction
2-Present day limitations and assumptions
3-Examples of applications
4-Imaging and 2D kernels
5-Non-uniform scattering
6-Depth dependance and the coupling of surface waves and body waves

Seismic fault imaging

Noise based tomography

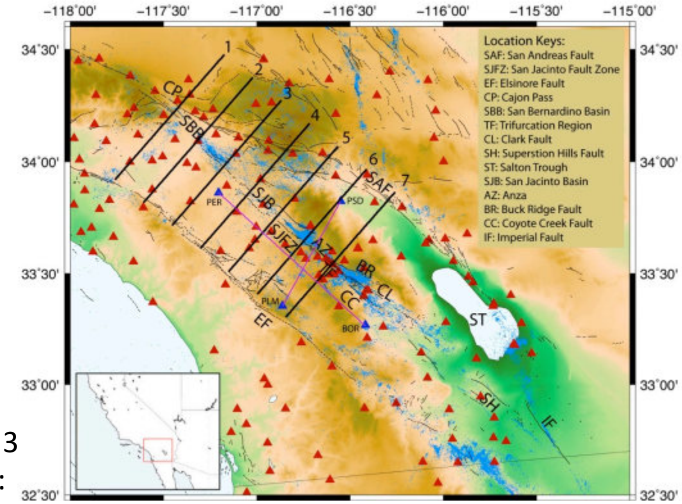

Station sismologique 3 composantes: NS/EW/Z

150 stations paires

9-component noise correlations

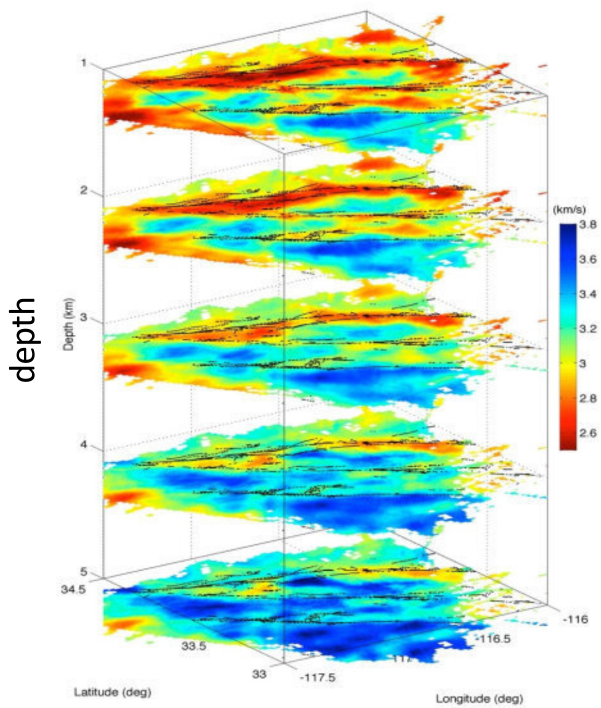

S-wave velocity image

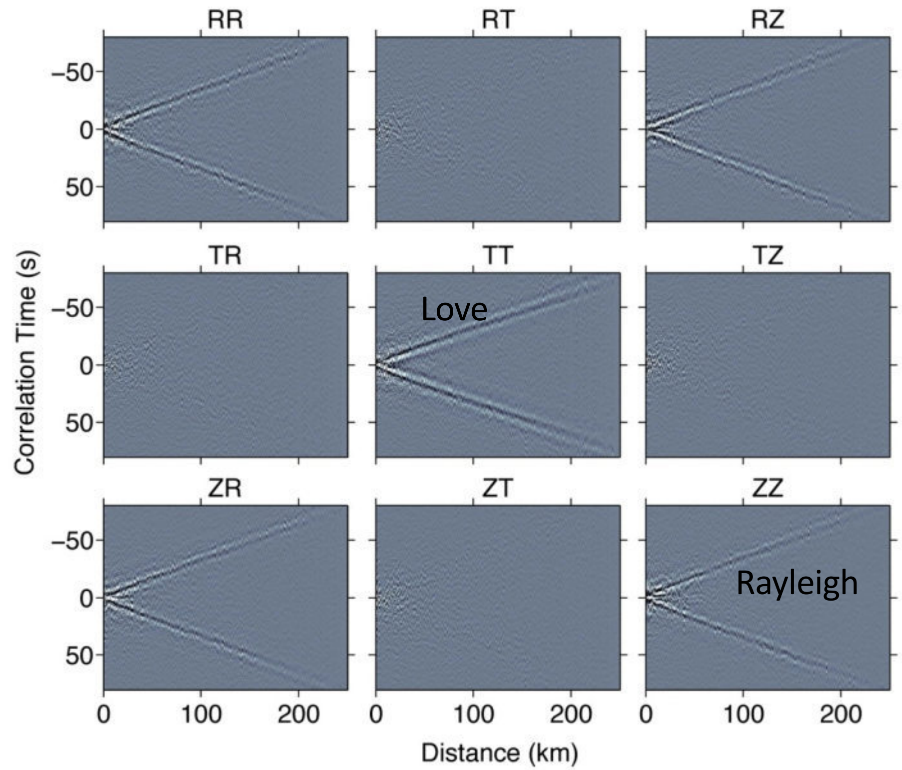

Zigone, et al., 2014

Scattering strength in the North Anatolian fault region based on observed intensity

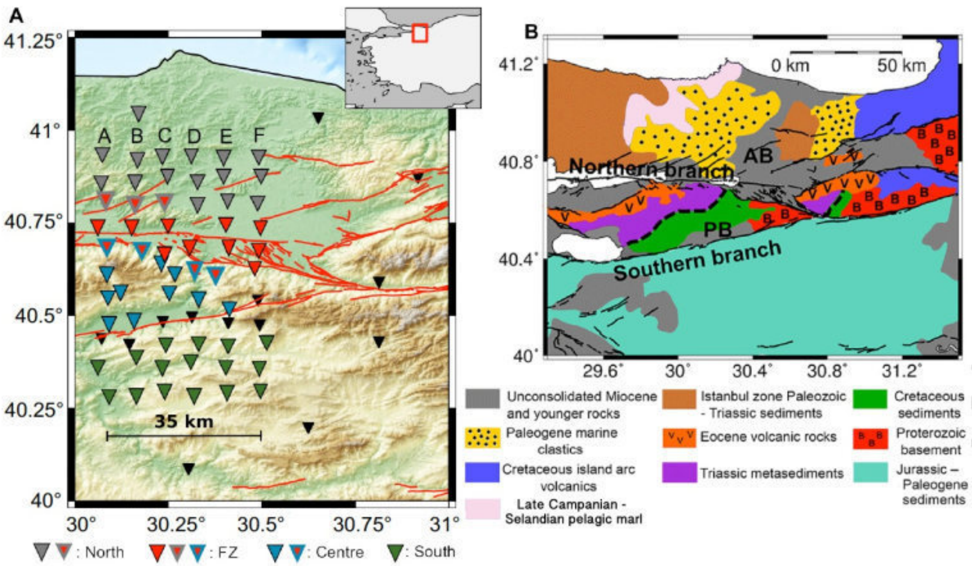

Coda intensity

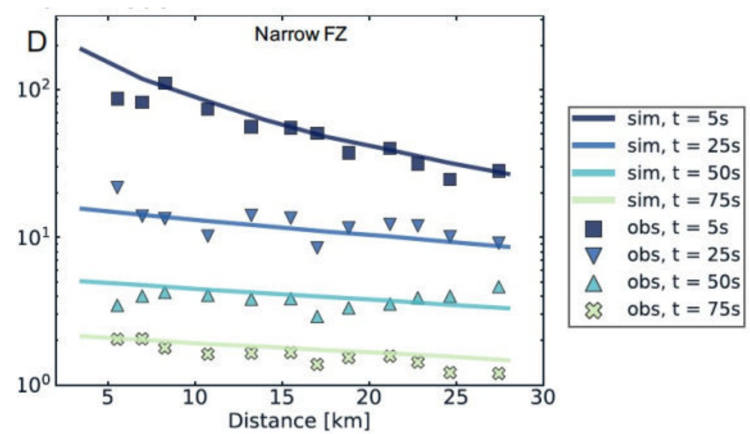

Data and Monte Carlo simulations in media with non-uniform scattering

➔ Existence of a narrow (around 5 km) high scattering zone along the Northern Branch of the NAF
(van Dinther et al, 2020)

Implications for monitoring/ sensitivity kernels?

Passive body wave imaging in the North Anatolian fault region

Matricial approach

Redatuming/backpropagation, beam forming + multiple scattering cancellation and iterative correction of aberrations (Aubry et al., Blondel et al., 2018, Touma et al. 2021a,b)

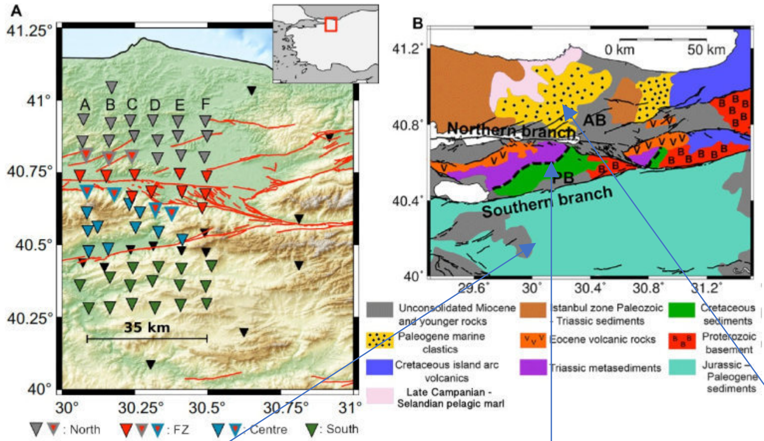

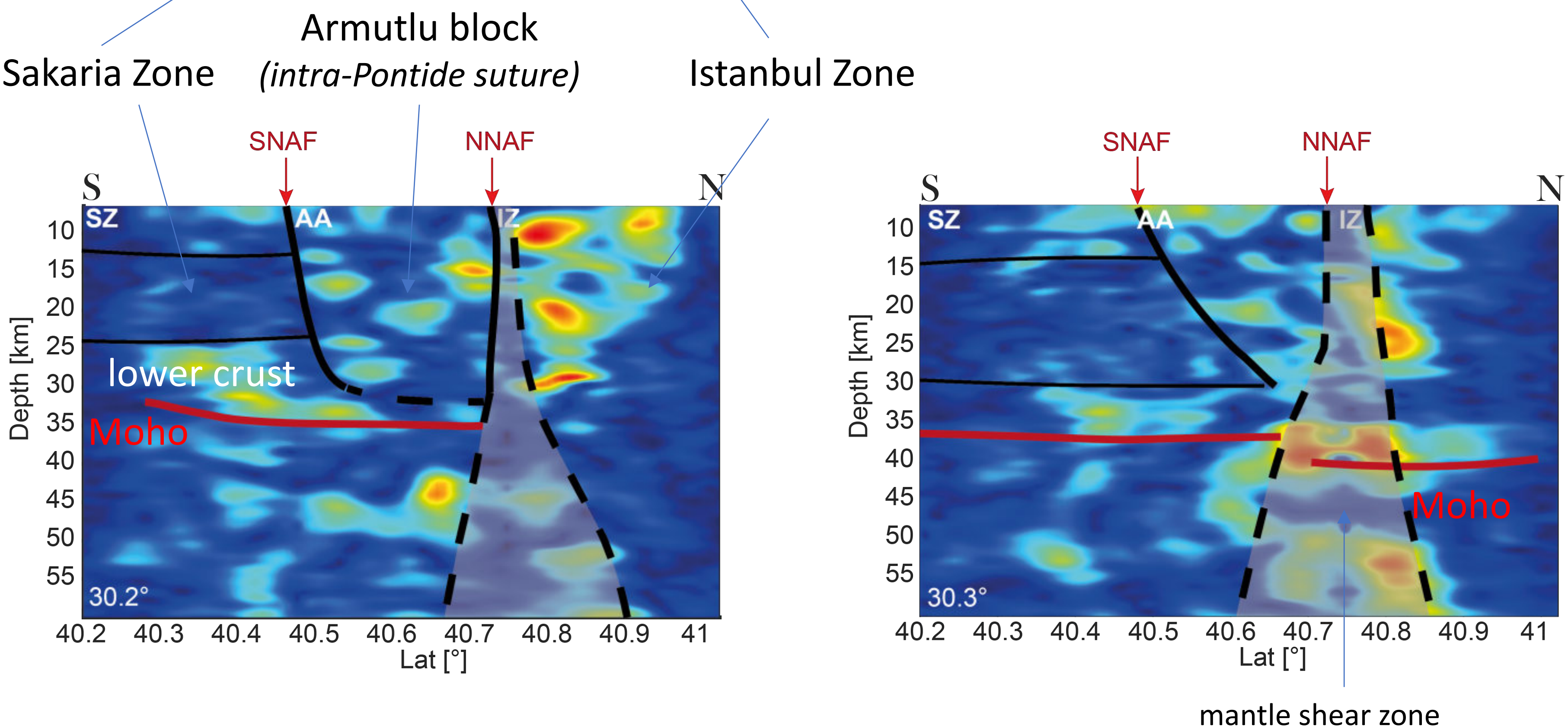

Numerical test : a velocity change in a section of the highly scattering North Anatolian fault

9 stations (noise correlations=sources and receivers)

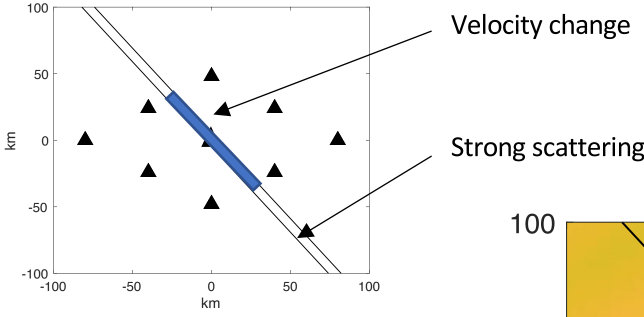

Inversion with a kernel computed for a model with uniform scattering properties

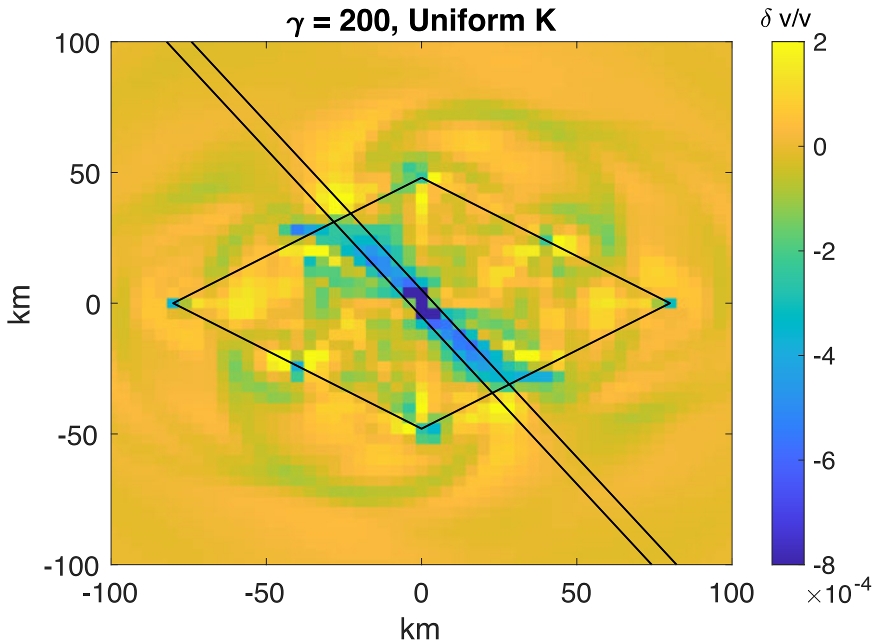

Kernels for medium where scattering properties are not uniform.
Monte Carlo simulations

$$K_{tt}\left(\mathbf{r}', t; \mathbf{r}, \mathbf{r}_0\right) = S^D \int_0^t \int_{S^D} \frac{I\left(\mathbf{r}', t-t', -\mathbf{n}'; \mathbf{r}\right) I\left(\mathbf{r}', t', \mathbf{n}'; \mathbf{r}_0\right) dt' dn'}{I\left(\mathbf{r}, t; \mathbf{r}_0\right)}$$

(van Dinther et al., 2021)

Fault zone (high scattering band)

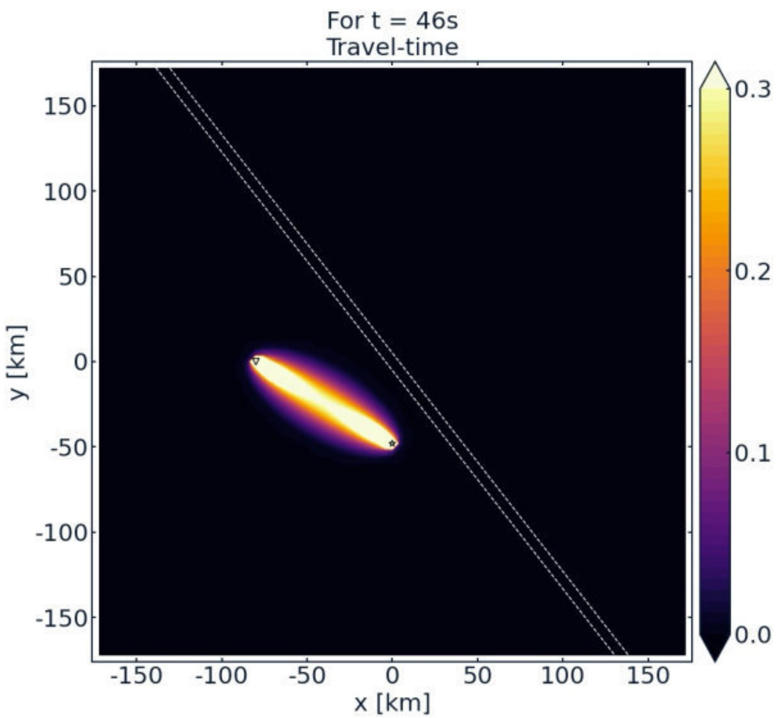

Numerical test : a velocity change in a section of the highly scattering North Anatolian fault

9 stations (noise correlations=sources and receivers)

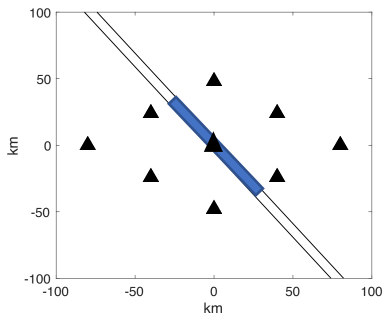

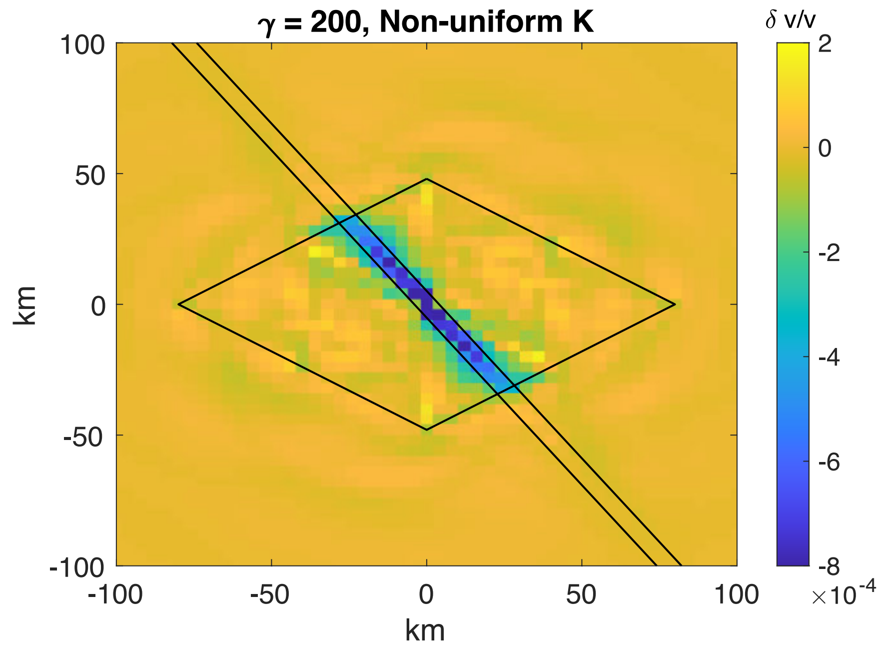

Inversion with a kernel computed for a model with non-uniform scattering properties

1-Introduction
2-Present day limitations and assumptions
3-Examples of applications
4-Imaging and 2D kernels
5-Non-uniform scattering
6-Depth dependance and the coupling of surface waves and body waves

Previous results on the coupling and sensitivity to a change in a thin flat layer

Numerical results of Obermann et al., 2016: full 3D elastic half space

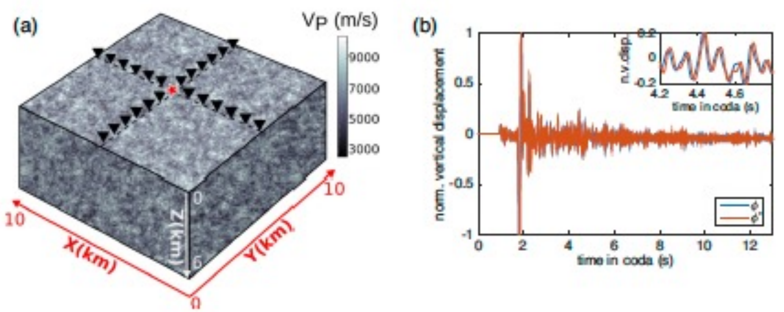

Figure 1. (a) Heterogeneous model (x, y) = 10 km, z = 6 km. The red star marks the source position and the black inverted triangles mark some exemplary receiver positions. (b) Synthetic seismograms recorded without (ϕ, blue) and with perturbed layer (ϕ', red) at the surface in a medium with 20 per cent velocity fluctuation.

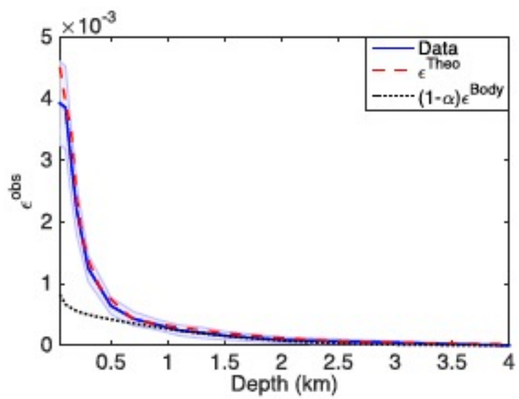

Figure 4. Apparent relative velocity changes with depth of the perturbed layer ($\sigma = 20$ per cent). The modelled data (dashed-red) $\varepsilon^{\mathrm{Theo}}(d, t = 2\ \mathrm{s})$ fit the observations very well. We note the importance of the surface waves, as the body-wave regime $(1-\alpha)\varepsilon^{\mathrm{Body}}$ (with $\alpha = 0.75$) alone cannot account for the steep slope at short times.

$$\varepsilon^{\mathrm{Theo}}(d,t) = \alpha(t)\varepsilon^{\mathrm{Surf}}(d) + (1-\alpha(t))\varepsilon^{\mathrm{Body}}(d,t).$$

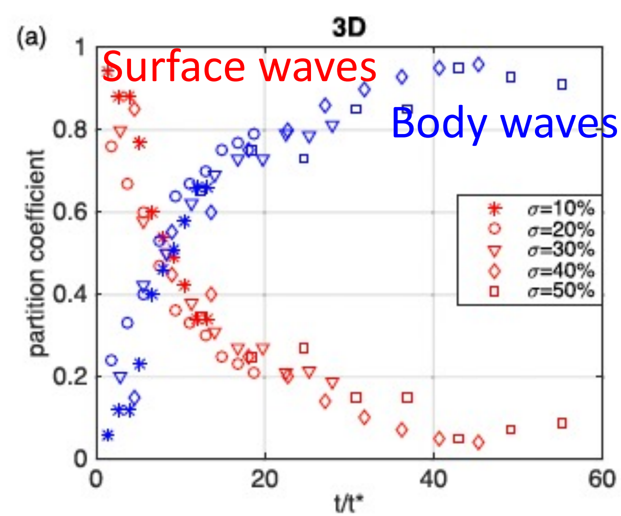

Scalar Wave Equation Model with Surface Waves

- Helmholtz Eq. with mixed B.C. in 3-D Half-Space geometry $(z > 0)$

$$\Delta u + \frac{\omega^2}{c^2} u = 0$$

Robin condition $\partial_z u + \alpha u = 0$ at $z = 0$ with $\overbrace{\alpha > 0}^{\text{penetration depth}^{-1}}$

- **Surface waves :** $u(\mathbf{r}, z) = \sqrt{2\alpha}\, e^{-\alpha z} \frac{e^{i\mathbf{k}_\parallel \cdot \mathbf{r}}}{2\pi}$ with $\underbrace{\mathbf{k}_\parallel \cdot \mathbf{k}_\parallel - \alpha^2 = \frac{\omega^2}{c^2}}_{\text{Dispersion relation}}$

Margerin, Barajas and Campillo (2019)

➔ Green function and (Born) differential cross sections

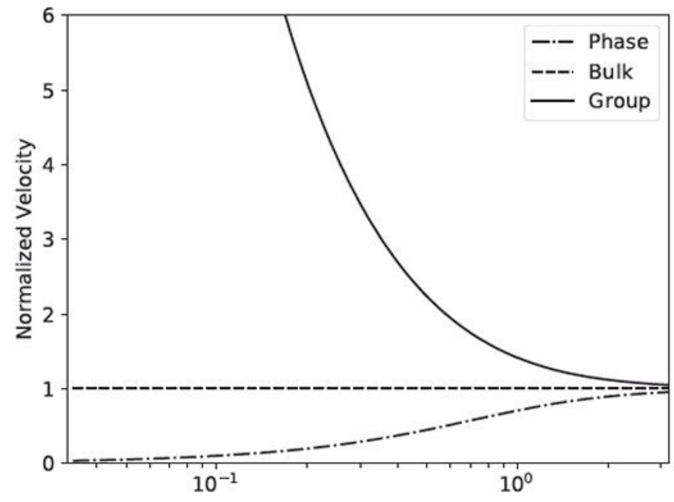

Transport Equation for coupled Surface and Body Waves

$$\left(\partial_t + v_g \widehat{\mathbf{n}} \cdot \nabla\right) e_s(t, \mathbf{r}, z, \widehat{\mathbf{n}}) = -\frac{e_s(t, \mathbf{r}, z, \widehat{\mathbf{n}})}{\tau^s} + \frac{1}{\tau^{s \to s}} \int_{2\pi} p^{s \to s}(\widehat{\mathbf{n}}, \widehat{\mathbf{n}}') e_s(t, \mathbf{r}, z, \widehat{\mathbf{n}}') d\hat{n}'$$
$$+ \boxed{\frac{1}{\tau^{b \to s}(z)} \int_{4\pi} p^{b \to s}(\widehat{\mathbf{n}}, \widehat{\mathbf{k}}') e_b(t, \mathbf{r}, z, \widehat{\mathbf{k}}') d\hat{k}'} + s_s(t, \mathbf{r}, z, \widehat{\mathbf{n}})$$

$$\left(\partial_t + c \widehat{\mathbf{k}} \cdot \nabla\right) e_b(t, \mathbf{r}, z, \widehat{\mathbf{k}}) = -\frac{e_b(t, \mathbf{r}, z, \widehat{\mathbf{k}})}{\tau^b(z)} + \frac{1}{\tau^{b \to b}} \int_{4\pi} p^{b \to b}(\widehat{\mathbf{k}}, \widehat{\mathbf{k}}') e_b(t, \mathbf{r}, z, \widehat{\mathbf{k}}') d\hat{k}'$$
$$+ \boxed{\frac{1}{\tau^{s \to b}} \int_{2\pi} p^{s \to b}(\widehat{\mathbf{k}}, \widehat{\mathbf{n}}') e_s(t, \mathbf{r}, z, \widehat{\mathbf{n}}') d\hat{n}'} + s_b(t, \mathbf{r}, z, \widehat{\mathbf{n}})$$

$$\text{B.C. : } e_b(t, \mathbf{r}, 0, \widehat{\mathbf{k}}_i) = e_b(t, \mathbf{r}, 0, \widehat{\mathbf{k}}_r)$$

Difference with Conventional Transport Equations

- Depth-Dependent Scattering Mean Free Time
- Surface Wave wavelength is a parameter in the Eqs

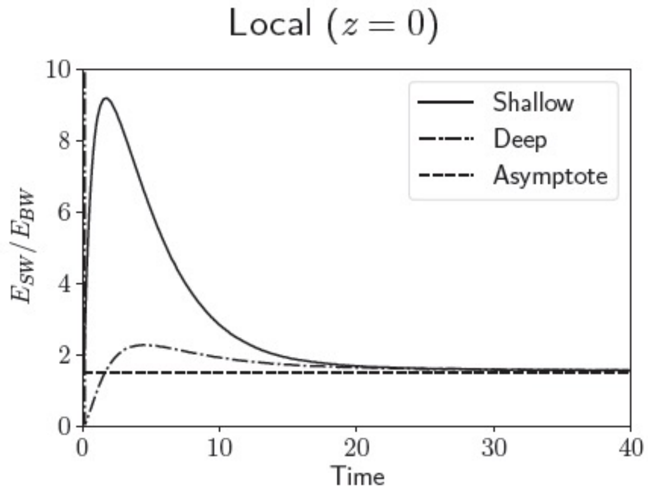

Energy Partitioning

Local partition at a fixed ratio (predominance of surface waves) as expected from the density of states

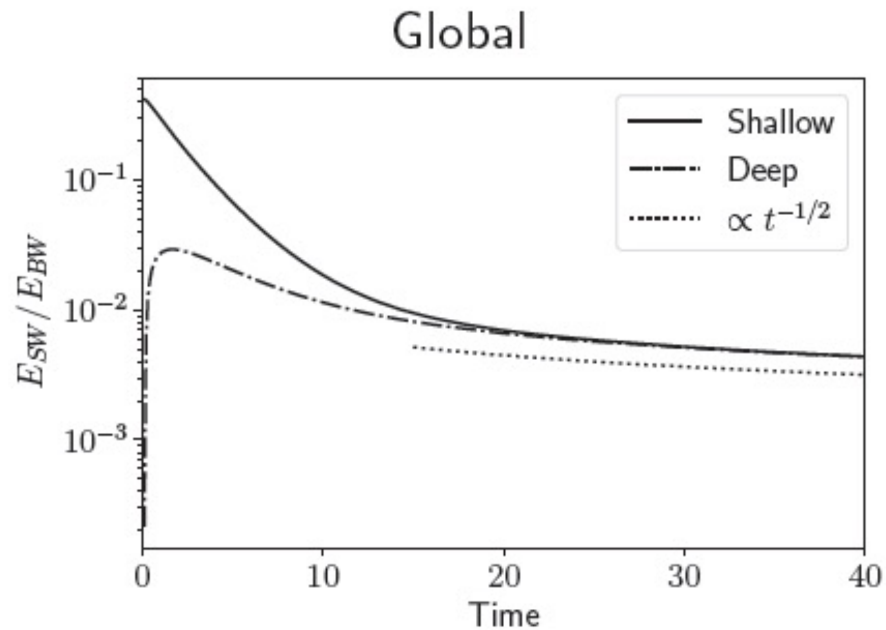

The ratio of global energies decays with time, even asymptotically as a signature of the dimensionality of the two wave processes.

The part of body waves in average in the medium increases with lapse time

Margerin, Barajas and Campillo (2019)

Probleme of a change in a flat layer. : the change depends only on depth

A phonon can propagate in two different modes, and can *also* arrive in two possible modes. We therefore can keep track of four different time densities

$$\bar{t}_{s\rightarrow s};\;\; \bar{t}_{s\rightarrow b};\;\; \bar{t}_{b\rightarrow s};\;\; \bar{t}_{b\rightarrow b} \tag{10}$$

First index: Propagation mode. Second index: Arrival mode.

Sensitivity Entanglement

This means that, for example, a particle that arrived propagating in the body wave mode could have been contributing to the sensitivity of the surface waves

$$\frac{\delta t}{t} = \int \left(-\frac{\langle t_s \rangle}{t} K_{C_{ph}}(z') - \frac{\langle t_b(z') \rangle}{t} \right) \frac{\delta c}{c}(z')\, dz'$$

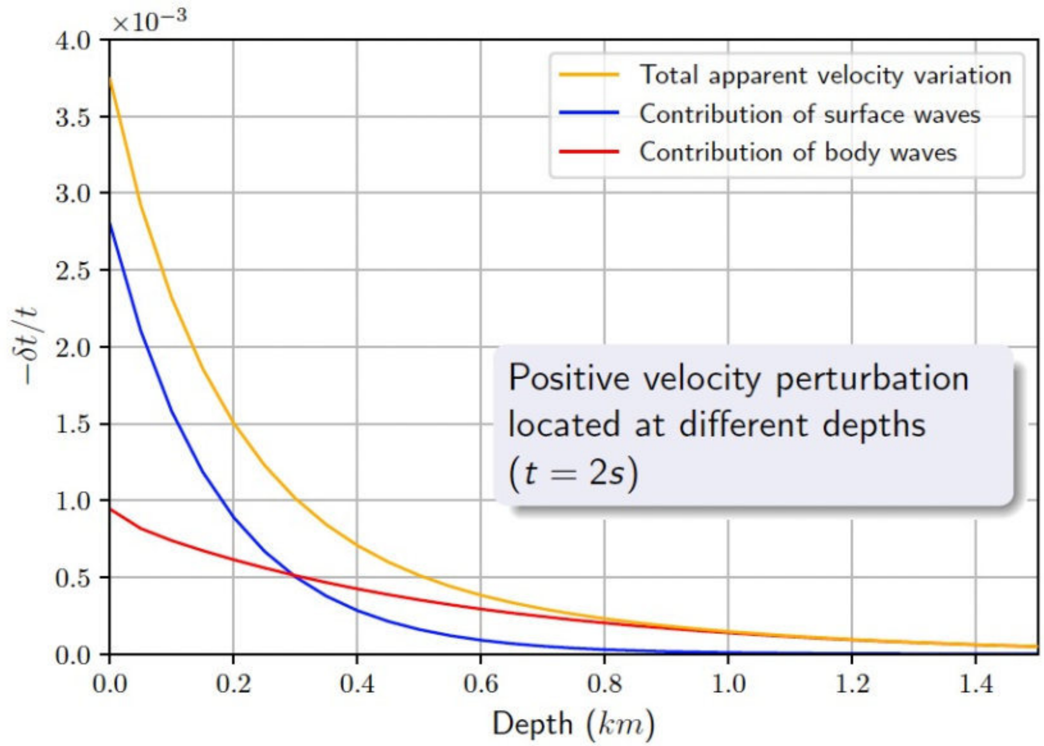

$$1 = \frac{\langle t_s(t,r,z)\rangle}{t} + \frac{\langle t_b(t,r,z)\rangle}{t} = \eta_s(t) + \eta_b(t)$$: Time partition coefficients

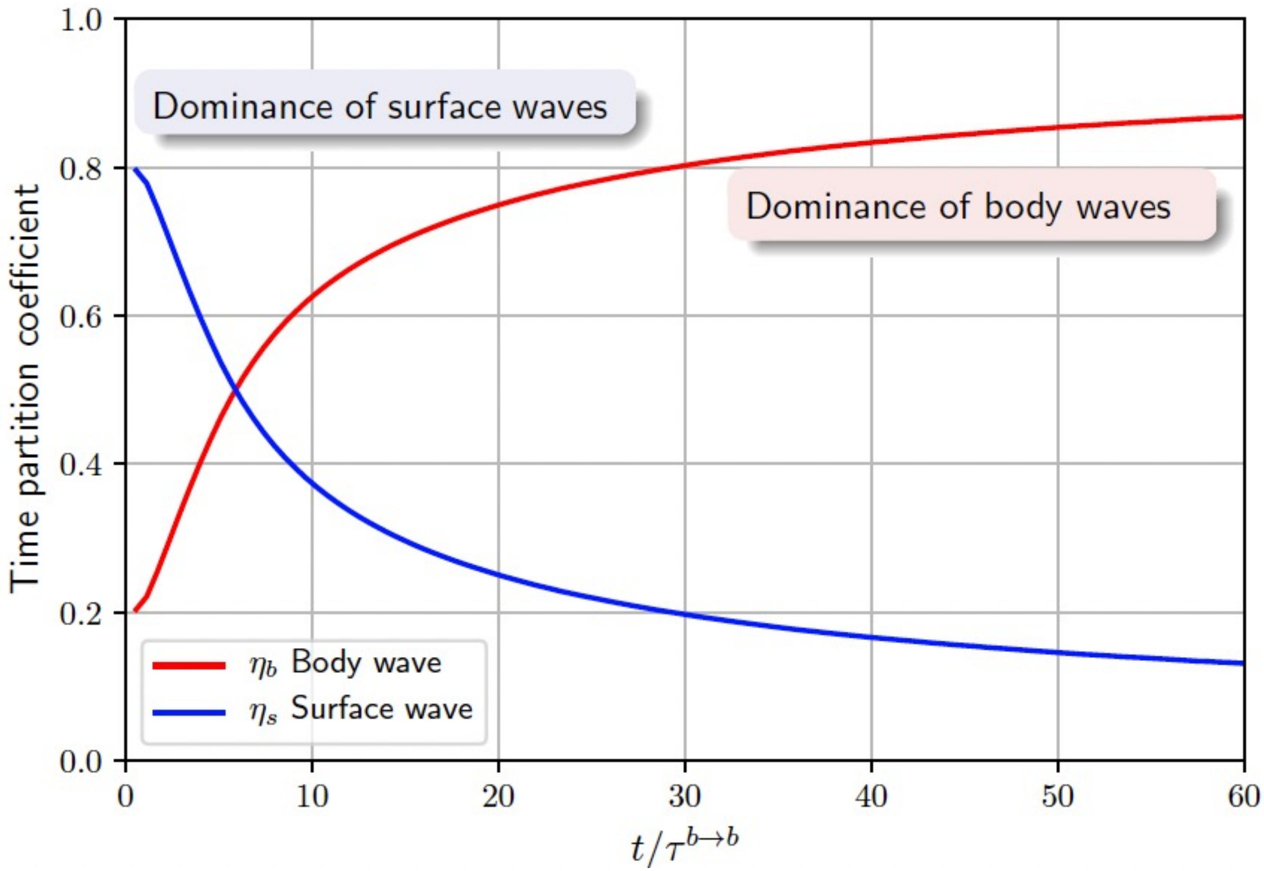

Time partition coefficient for body waves

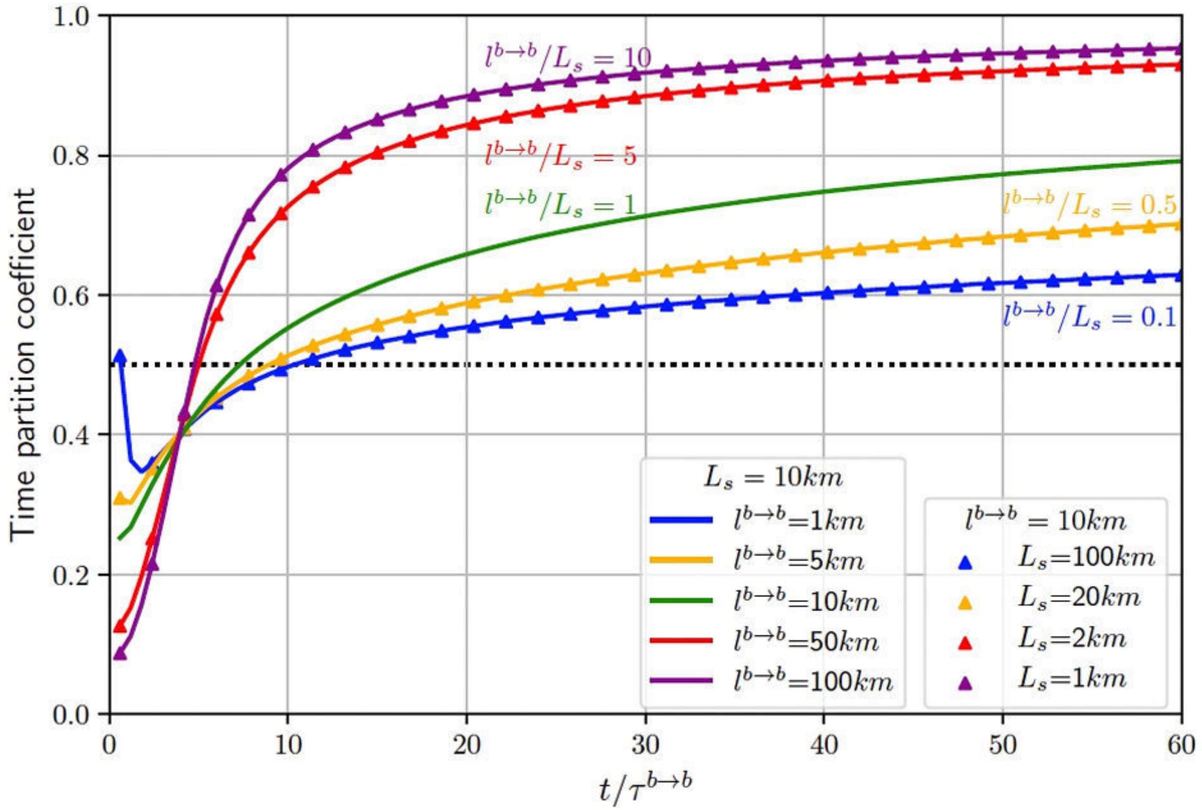

L_s: penetration depth of surface waves ≃ wave length

l mean free path

The sensitivity of the system is completely controlled by the ratio $l^{b\to b}/L_s$

➔ *frequency dependent*

➔ *towards a full 3D coupled kernel*

Short conclusion

Measure of dt(t) with scattered waves …

Importance of a good knowledge of the structure (velocity AND scattering)…

Importance of including body to surface wave coupling in 3D at least at a first order…